OPTICA

GHz repetition rate mid-infrared frequency comb spectroscopy of fast chemical reactions

Nazanin Hoghooghi,[1,2,†,*] Peter Chang,[3,4,†] Scott Egbert,[1] Matt Burch,[5] Rizwan Shaik,[5] Scott A. Diddams,[3,4,6] Patrick Lynch,[5] and Gregory B. Rieker[1]

[1]Precision Laser Diagnostics Laboratory, University of Colorado, Boulder, Colorado 80309, USA
[2]Current address: Time and Frequency Division, National Institute of Standards and Technology, Boulder, Colorado 80305, USA
[3]Time and Frequency Division, National Institute of Standards and Technology, Boulder, Colorado 80305, USA
[4]Department of Physics, University of Colorado, Boulder, Colorado 80309, USA
[5]Department of Mechanical and Industrial Engineering, University of Illinois Chicago, Chicago, Illinois 60607, USA
[6]Electrical, Computer and Energy Engineering Department, University of Colorado, Boulder, Colorado 80309, USA
[†]These authors contributed equally to this work.
*nazanin.hoghooghi@colorado.edu

Received 15 February 2024; revised 22 April 2024; accepted 11 May 2024; published 17 June 2024

Molecular diagnostics are a primary tool of modern chemistry, enabling researchers to map chemical reaction pathways and rates to better design and control chemical systems. Many chemical reactions are complex, involving multiple species and reaction pathways occurring on μs or shorter timescales. Existing diagnostic approaches provide a subset of chemical and thermodynamic information. Here we optimize across many diagnostic objectives by introducing a high-speed and broadband, mid-infrared dual-frequency-comb absorption spectrometer. The optical bandwidth of $>1000\ cm^{-1}$ covers absorption fingerprints of many species with spectral resolution $<0.03\ cm^{-1}$ to accurately discern their absolute quantities. Key to this advance are 1 GHz pulse repetition rate mode-locked frequency combs covering the 3–5 μm region that enable a spectral acquisition rate of $290\ cm^{-1}$ per 17.5 μs per detector for *in situ* tracking of fast chemical process dynamics. We demonstrate this system to quantify the abundances and temperatures of each species in the complete reactants-to-products breakdown of 1,3,5-trioxane, which exhibits a formaldehyde decomposition pathway that is critical to modern low-temperature combustion systems. By maximizing the number of observed species and improving the accuracy of temperature and concentration measurements, this spectrometer provides a pathway for modern chemistry approaches such as combining chemical models with machine learning to constrain or predict complex reaction mechanisms and rates.

https://doi.org/10.1364/OPTICA.521655

1. INTRODUCTION

Better understanding of chemical reaction pathways and rates has enabled large gains in transportation fuel efficiency, lower-emission chemical manufacturing, improved fire suppression, and hypersonic propulsion, among other innovations. Oversimplification or oversight with respect to even minor pathways can have negative implications on models and their macroscopic predictions of reaction behavior, as recently observed with roaming reactions, termolecular reactions, and non-thermal prompt reactions [1–4]. Controlled chemical reactors together with *in situ* diagnostics are key to improving understanding of these pathways. An ideal *in situ* diagnostic approach would reveal the complex reaction pathways and kinetic rates by (1) probing *as many* critical chemical species from reactants to products as possible, (2) with high specificity and concentration accuracy, (3) at the timescales of the reaction (e.g., microseconds at combustion temperatures).

Here we introduce and demonstrate a dual-frequency-comb absorption spectrometer that achieves these three desirable characteristics for chemical kinetic diagnostics. Our spectrometer provides broad optical bandwidth to measure the mid-infrared absorption fingerprint of complex molecular reactants. Simultaneously, it has high spectral resolution to accurately distinguish small intermediate and product species and rotational/vibrational temperatures. It also accomplishes all of this on microsecond timescales.

The invention of broad optical bandwidth mode-locked frequency combs opens new potentials for accurate, multi-species laser-based diagnostics. Quantum transitions in many molecules can be probed simultaneously with thousands of finely spaced and precisely known optical frequencies that are individually measured at comb tooth resolution by interfering two combs together, a technique called dual-comb spectroscopy (DCS) [5,6]. DCS breaks the size/acquisition-rate/resolution limitations of the Fourier transform spectrometers (FTSs) that have been a workhorse of optical

absorption sensing for decades, replacing the mechanical scanning arm of the FTS Michelsen interferometer with the motionless interference of the two frequency combs.

However, several fundamental tradeoffs of frequency comb properties (e.g., tooth spacing, pulse power) make it challenging to perform DCS over a broad optical bandwidth with high resolution at the appropriate acquisition speed needed to study many physical processes. The maximum optical bandwidth ($\Delta\nu$) achievable with DCS for a given acquisition time (τ_{ac}) when using one photodetector and the full interferogram is given by $\Delta\nu/\tau_{ac} \leq f_{rep}^2/2$, where f_{rep} is the spacing between comb modes (equivalent to the pulse repetition rate of the comb-generating laser) [6] (noting that parallel acquisition by multiplexing N spectrally filtered bands to N photodetectors increases the total DCS bandwidth by N). Larger frequency comb mode spacing greatly improves bandwidth. However, without interleaving, the point spacing of the resultant spectrum decreases with higher mode spacing. In addition, not all frequency comb architectures are able to generate light across the full detectable optical bandwidth given by the equation above. This issue is visualized in Figs. 1(a)–1(d) for the three primary *mid-infrared* frequency comb architectures. Quantum cascade and interband cascade frequency combs (QCL/ICL) have 10+ GHz comb mode spacing that achieves high acquisition speed and high power-per-mode, though with limited single-shot resolution and optical bandwidth [7–11]. Electro-optic modulator combs can have narrow mode spacing (e.g., 300 MHz) to achieve high resolution, but with limited optical bandwidth [12–15]. Finally, mode-locked combs that generate large mid-infrared optical bandwidth do so with a lower pulse repetition rate to maintain high pulse power to drive the nonlinear optical processes that create the bandwidth [16–23], with the exception of recent sources based on Cr:ZnS mode-locked lasers [24,25]. Figure 1(e) compares the performance of several of the existing mid-infrared dual-comb spectrometers used for gas phase spectroscopy experiments. We note that several high-repetition-rate dual-comb spectrometers have also been demonstrated in the near-infrared wavelength region [26–30].

The spectrometer described here is enabled by mode-locked frequency combs that achieve both broad bandwidth and high power-per-comb-mode in the mid-infrared at 1 GHz pulse repetition rates using chirped pulse amplification and a robust intra-pulse difference frequency generation technique [21,31]. The spectrometer continuously spans the entire C-H stretch rovibrational energy range (3–5 μm, >1000 cm^{-1}), spectral point spacing of 0.03 cm^{-1} (1 GHz), and acquisition rate of up to 290 cm^{-1} per 17.5 μs per detector. This is the maximum DCS bandwidth for $\tau_{ac} = 17.5$ μs and $f_{rep} = 1$ GHz as described in the DCS equation above. Thus, the full 1000 cm^{-1} bandwidth (~30,000 comb modes, >50 nW per comb mode) can be measured at a time resolution of 60 μs with a single detector. Or alternatively, different portions of the spectrum can be measured with faster time resolution using multiple detectors, as demonstrated in this paper. The 1 GHz mode spacing and broad

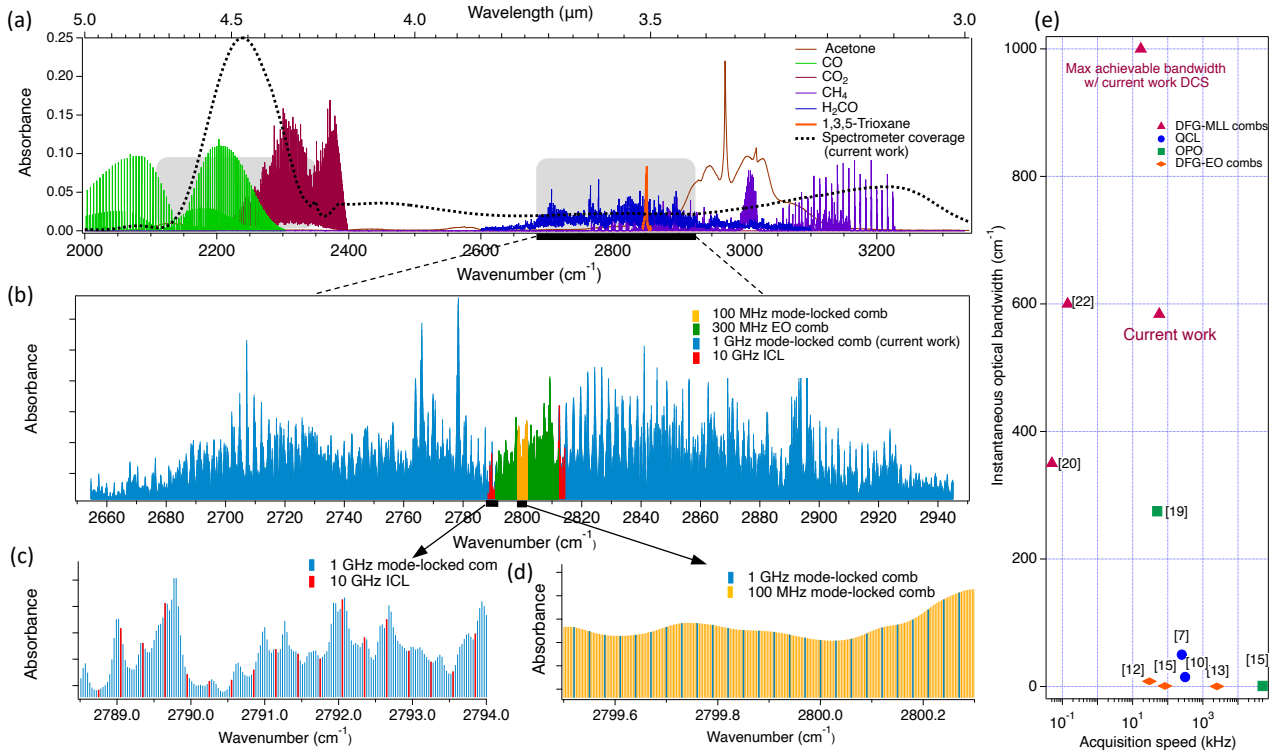

Fig. 1. Comparing mid-infrared frequency comb spectrometers. (a) Continuous span of the 1 GHz repetition rate dual-comb spectrometer introduced in this study (dashed line) with example underlying molecular absorption spectra. The two shaded regions of the spectrum are simultaneously acquired in 17.5 μs by the two-detector configuration of this study. (b) Span of the formaldehyde absorbance spectrum that can be acquired in 10 μs in dual-comb configuration for various mid-infrared frequency comb architectures. Different colors indicate the maximum demonstrated bandwidth by a dual-comb mid-infrared spectrometer at 100 MHz, 300 MHz, 1 GHz, and 10 GHz repetition rates (comb tooth spacings). At bottom are zoomed insets of the single-shot spectral resolution possible with various mid-infrared dual-comb architectures: (c) 1 GHz versus 10 GHz dual-comb spectrometer and (d) 1 GHz versus 100 MHz dual-comb spectrometer. Note that the vertical lines indicate the spectral sampling by the spectrometer (i.e., each vertical line represents a sample). (e) Instantaneous optical bandwidth versus acquisition speed of some of the existing mid-infrared dual-comb spectrometers.

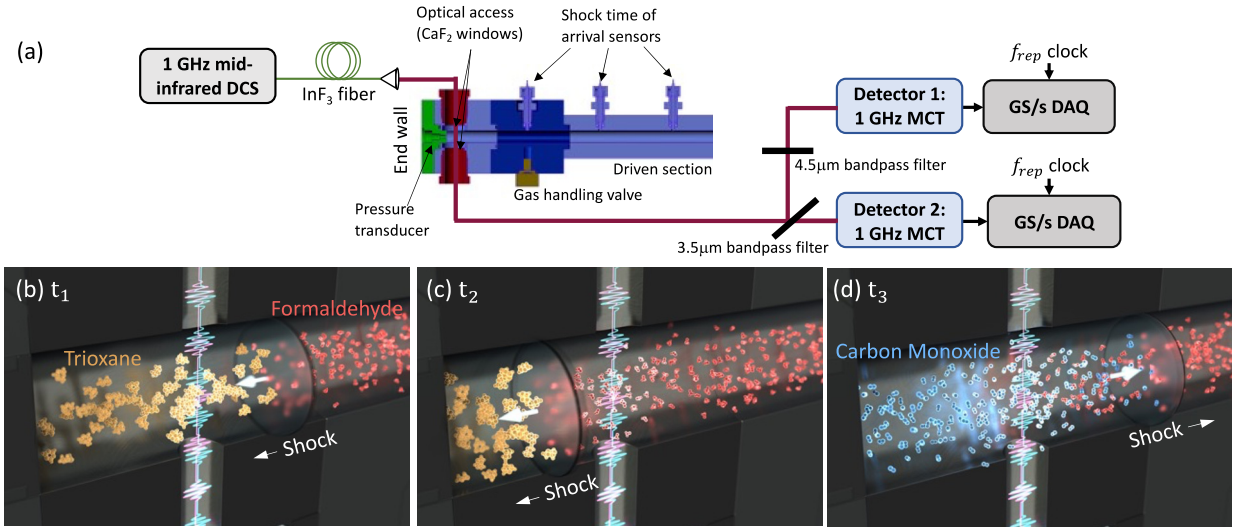

Fig. 2. Experimental setup. (a) Experimental schematic. The incident shock travels from right to left in this view. From the right, the shock passes across time-of-arrival sensors to measure the shock velocity. The dark blue section is a custom valve, which opens the tube to evacuate the driven section after each experiment. Next, there is a window section (light blue) with CaF_2 windows held in by retaining nuts (red). The laser traverses the tube through this window section. Finally, the shock tube has an endwall (green) instrumented with a pressure transducer. (b)–(d) Pulses from two mid-infrared frequency combs (colored differently for clarity) are propagated collinearly for dual-comb spectroscopy through optical access close to the shock tube endwall. The dissociation of trioxane (yellow) into intermediate formaldehyde (red) and product carbon monoxide (blue) is initiated by (b), (c) the passage of an incident and (d) reflected shock wave.

bandwidth can resolve most molecular species at the temperatures, pressures, and timescales of reacting systems, particularly as multiple detectors are employed.

With this capability, we study the decomposition of 1,3,5-trioxane ($C_3H_6O_3$) to formaldehyde (H_2CO), and formaldehyde's subsequent reactions to carbon monoxide (CO) in a high-repetition-rate shock tube [32]. Formaldehyde is known to be a critical intermediate species in low-temperature combustion *en route* to ignition [33–36]. The strong endothermicity of the precursor decomposition further complicates this system, which leads to uncertainty in rate constants from the uncertain temperature assignment following the decomposition of the precursor [10,37]. We simultaneously measure time-resolved concentrations of molecular reactants, smaller intermediates (H_2CO), products (CO), and the gas temperature throughout the reaction with high accuracy and 17.5 μs time resolution. Quantitatively tracking an array of molecular species and including temperature constrains reaction pathways and rates. This molecular "cinema" can provide new insight into a host of kinetic research challenges.

2. EXPERIMENT

Among the mid-infrared frequency comb architectures, mode-locked combs have demonstrated the broadest optical output bandwidth due to the ability to leverage high peak pulse power to drive nonlinear frequency generation and conversion processes. However, mid-infrared mode-locked combs have thus far been demonstrated at pulse repetition rates ≤ 200 MHz with a few exceptions in Cr:ZnS [24,25], which limits the DCS bandwidth to 6.7 cm^{-1}/10 μs–enough to probe only a single absorption transition of a small molecule at microsecond timescales. Here we improve the optical bandwidth by two orders of magnitude, enough to measure overlapping spectra of multiple large and small molecules at microsecond timescales, by creating a mid-infrared dual-frequency-comb spectrometer with 1 GHz repetition rate. Increasing the repetition rate reduces peak pulse power (for a given average laser power), which hinders the nonlinear processes. The spectrometer is made possible by the generation of sub-two cycle (8 fs) pulses at 1 GHz repetition rate, centered at 1.56 μm with ∼0.25 MW peak power [31], which efficiently drives the intra-pulse difference frequency generation (IP-DFG) processes to generate the broadband mid-infrared frequency comb. We generate these pulses using chirped pulse amplification (CPA) and soliton self-compression in an anomalous dispersion highly nonlinear fiber [38]. These pulses then drive the IP-DFG inside an $\chi^{(2)}$ nonlinear crystal to generate mid-infrared light. We use a fan-out periodically poled lithium niobate (PPLN) crystal. The result is a broadband 1 GHz MIR frequency comb, with >4 mW of power and continuous coverage of the entire 3–5 μm region. Both GHz frequency combs are fully stabilized using FPGA-based lock continuous coverage of the entire 3–5 μm region. Both GHz frequency combs are fully stabilized using FPGA-based lock boxes with ∼100 kHz bandwidth for both optical and f_{ceo} locks. This enables simple phase correction, followed by coherent averaging of the dual-comb signal (see Supplement 1).

The acquisition rate of the spectrometer is defined by the difference between the repetition rates of the two frequency combs and can be adjusted from a few Hz up to 100 kHz (the limit of the piezo actuator range that adjusts the cavity length of the near-infrared oscillator). After passing through the experiment, we split and bandpass filter the frequency comb light into two wavelength regions, each passed to a separate detector [Fig. 2(a)]. This doubles the optical bandwidth for a given acquisition rate [39], and improves the SNR by reducing the bandwidth of light on each detector to provide more power-per-comb-mode before detector saturation [40]. Interferograms are collected using a FPGA- based data acquisition card, sampling the interferogram at the pulse repetition rate (1 GHz).

We use a small-diameter high-repetition-rate shock tube for the studies [32,41] (Fig. 2). The opening of a high-speed valve

separating a low-molecular-weight high-pressure driver gas and high-molecular-weight low-pressure driven gas propagates a shock wave down the tube. The shock wave increases the temperature of the driven gas, and after reflecting from the endwall of the tube, propagates through the gas again, further increasing the gas temperature to values as high as 1700 K in these experiments.

We collect an interferogram that represents a full comb-tooth-resolved spectrum every 17.5 μs during 800 consecutive shocks collected over 53 min. We ensemble average all of the repeated shock events to optimize the signal-to-noise ratio given the short pathlength and small absorbance present in these experiments. Interferograms are aligned and binned relative to the reflected shock, and each bin is phase corrected and averaged together to reach a noise-equivalent-absorbance ranging from 1×10^{-5} to 2×10^{-5} (depending on spectral region) according to the formula [42] $\mathrm{NEA} = (L \times \mathrm{SNR})^{-1} \times (\frac{T}{M})^{\frac{1}{2}}$, where L is the absorption pathlength, T is time, and M is the number of spectral elements (comb teeth). Vacuum scans of the empty shock tube were taken at the start of each day of testing to characterize the laser baseline and normalize subsequent measurements. No significant variations were observed throughout the test campaign.

3. RESULTS

We determine gas temperature by comparing the measured CO absorption from 24 rotational transitions of the fundamental vibrational band to the equilibrium Boltzmann distribution. This comparison avoids the influence of lineshape and linestrength errors in molecular absorption databases, which are common at these high temperatures (see Supplement 1). This method is uniquely available to this spectrometer, which has the optical bandwidth to cover a rotational manifold of CO with high enough resolution to fully resolve each transition.

We quantify species concentrations for CO and H_2CO by fitting a HITRAN2020-based model to the broadband data using the mFID approach [43], shown in Fig. 3, at the measured rotational temperature. The HITRAN2020 database [44] does not include collision-broadening parameters for CO or H_2CO with argon (which makes up over 90% of the mixture in the shock tube). Additional shock tube measurements were taken of a known mixture of CO ($5.02 \pm 0.10\%$) in argon at comparable conditions to the trioxane shocks to assess the impact of the unknown parameters on the retrieved concentration. The spectrometer retrieved a concentration of $5.01 \pm 0.33\%$ using HITRAN2020 across all conditions, indicating that there is no discernable concentration bias due to this shortcoming of the database. This resilience to database error also likely stems from the bandwidth of the spectrometer, which allows the fit to optimize over a large number of transitions with different linestrengths rather than just one. We did not quantify the transient intermediate species HCO or CH_2OH as their concentration does not exceed 50 ppm throughout the reaction. Future implementations of this system using cavity enhancement could enable such low-concentration species to be measured [45].

A quantitative reference absorption cross section is not available for trioxane. Instead, 2 ms of DCS data of the stable pre-shock period when trioxane is present and stable were averaged together to create a reference spectrum, and the pre-shock trioxane concentration value was determined from detailed balance between the trioxane concentration before the shock and the CO concentration 1 ms after the shock (when H_2CO was completely consumed). The reference spectrum was then used to fit the time-resolved data during the reaction, creating a relative measurement of trioxane concentration.

We perform four sets of experiments at different temperature, pressure, and precursor conditions to inform the analysis (see Supplement 1). In the experiments, dissociation of trioxane creates formaldehyde, which subsequently dissociates to carbon monoxide. A small amount of iodoethane is added to the initial mixture in some experiments to attempt to isolate H radical abstraction reactions. However, all experiments were already sensitive to bimolecular reactions because of the relatively high initial concentration of trioxane.

Figure 4 shows the measured temperature, concentration, and pressure values from one set of experiments. Typically, in shock tube studies, the reaction temperature is assumed to be a constant value calculated from ideal normal shock relations, or experimentally calibrated using a chemical thermometer (observation of a well-known chemical reaction over a well-defined time). There are several reasons for deviations of temperature from the ideal relations including boundary layer formation and reaction exo- or endothermicity in non-dilute systems. Thus, a spectroscopic measurement of temperature is preferred in all but the most ideal shock tube experiments (large diameter tubes, low dilution, etc.), and is occasionally performed. Here we use a small diameter tube and 2% trioxane in Ar mixture, with $\Delta \mathrm{Hr} > 35$ kcal/mol for the initial decomposition (not considered a dilute mixture), so the spectroscopic approach is more accurate. Indeed, in this experiment the spectroscopically measured temperature is necessary, as shown by the difference between the spectroscopically measured temperature and the estimate by the frozen normal shock relations.

We create a model of the system, where we fit the chemical kinetic model to the concentration of formaldehyde (H_2CO), CO, and the spectroscopically measured temperature. The model uses a custom pressure-dependent reactor (endwall transducer measured pressure) based on a method employed by Tang and Brezinsky [46]. The Aramco 3.0 kinetic database [47] serves as the base mechanism with the few modifications that are highlighted below and in Supplement 1. The model is shown in solid black line in Fig. 4. Note that the model trace shown in Fig. 4 is smoothed to the same time resolution of the measurement to enable easier comparison. The CO concentration plateaus before the temperature begins to decrease, suggesting that the reaction is complete. The temperature measurement agrees within uncertainty with the modeled temperature trace through the peak temperature until the end of the test time (80% of peak pressure). Excellent agreement between the modeled and experimental H_2CO and CO mole fraction traces is achieved using the updated chemical kinetic model.

The chain propagating reaction $\mathrm{HCO} + \mathrm{M} \rightarrow \mathrm{H} + \mathrm{CO} + \mathrm{M}$ [(R3) in Supplement 1] and chain terminating reaction $\mathrm{HCO} + \mathrm{H} \rightarrow \mathrm{H_2} + \mathrm{CO}$ [(R6) in Supplement 1] of the HCO radical are typically very fast and compete, influencing the rate of conversion of H_2CO to CO. The composition of H_2CO and CO is most sensitive to reaction (R3) [Fig. 5(a)], and its rate is adjusted and reported for all four sets of experiments in Fig. 5(b). While high sensitivity does not imply high uncertainty in rate constant assignment, in the case of this system, past measurements of the reaction rate for R3 are uncertain. As shown in Fig. 5, our measurements agree with past determinations of the reaction rate for R3

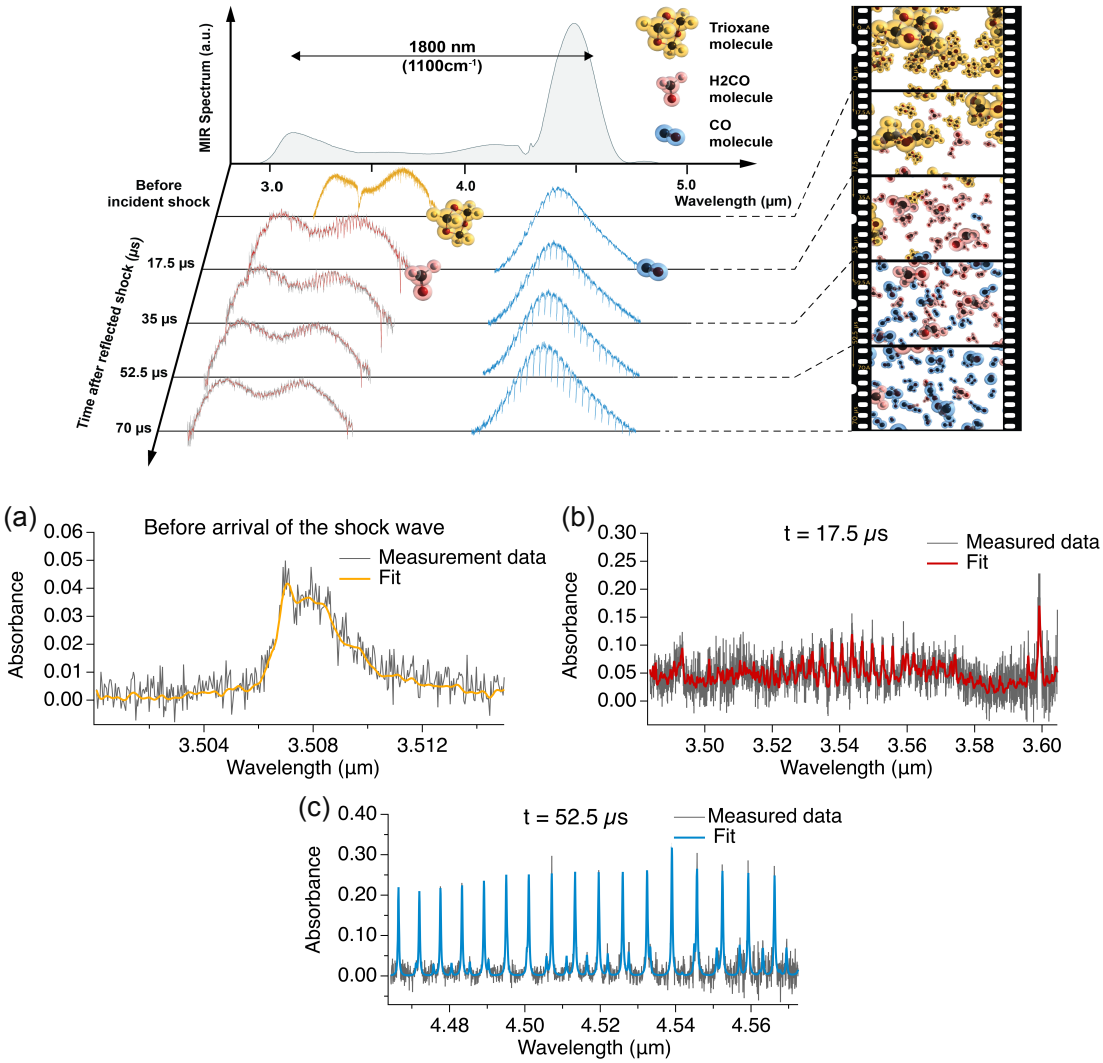

Fig. 3. Breakdown of 1,3,5 trioxane captured by dual-comb spectroscopy: (top) mid-infrared laser output spectrum taken with two detectors (linear scale) spanning 1800 nm across the trioxane, formaldehyde, and carbon monoxide absorption bands. The transmission spectrum of trioxane before the arrival of the shock wave and the two transmission spectra in subsequent frames are recorded with 17.5 μs time steps (57 kHz repetition rate detuning) and are shown after bandpass filtering and separate detection. The retrieved concentration and temperature create a molecular "cinema," as the intermediate formaldehyde (detected at $\lambda_c \sim 3.5$ μm) is depleted to form the product carbon monoxide (detected at $\lambda_c \sim 4.5$ μm). (bottom) (a) Example of the averaged absorption spectra collected for trioxane before arrival of the reflected shock wave, (b) H_2CO 17.5 μs after the reflected shock wave, and (c) CO 52.5 μs after the reflected shock wave together with fit to the data.

and agree with the rate chosen for the recently reported Aramco 3.0 mechanism [47].

Measurements of multiple species can provide additional observables to constrain the series of reactions from precursors to products. We show that measuring both species and temperature moderately lowers the uncertainty in assigning rate constants for the important reaction R3 (see Supplement 1) [29,41].

In addition, there is an ever-growing presence of large data analytic tools, such as machine learning, that are being applied to complex processes including chemistry. For chemical kinetics, these tools benefit from optimization against many observables [48]. Frequency combs offer a bridge between observable-rich mass spectrometry that has been applied in machine learning approaches, and the few species but quantitative and time-resolved nature of laser absorption spectrometry, as recently demonstrated for disease detection [49]. Achieving both speed and multi-species discrimination, this spectrometer opens the door to new machine learning advances in high-speed chemistry.

4. CONCLUSION

In summary, we demonstrate a dual-comb spectrometer that enables *in situ* speciation and thermometry for microsecond timescale molecular reactions. The spectrometer achieves a balance of high bandwidth, spectral resolution, and acquisition rate by leveraging the first 1 GHz repetition rate mid-infrared mode-locked combs. The combs combine chirped pulse amplification with IP-DFG to enable sufficient peak pulse power to generate spectra across more than 1000 cm^{-1} of the chemically important 3–5 μm spectral absorption range. We use the spectrometer to

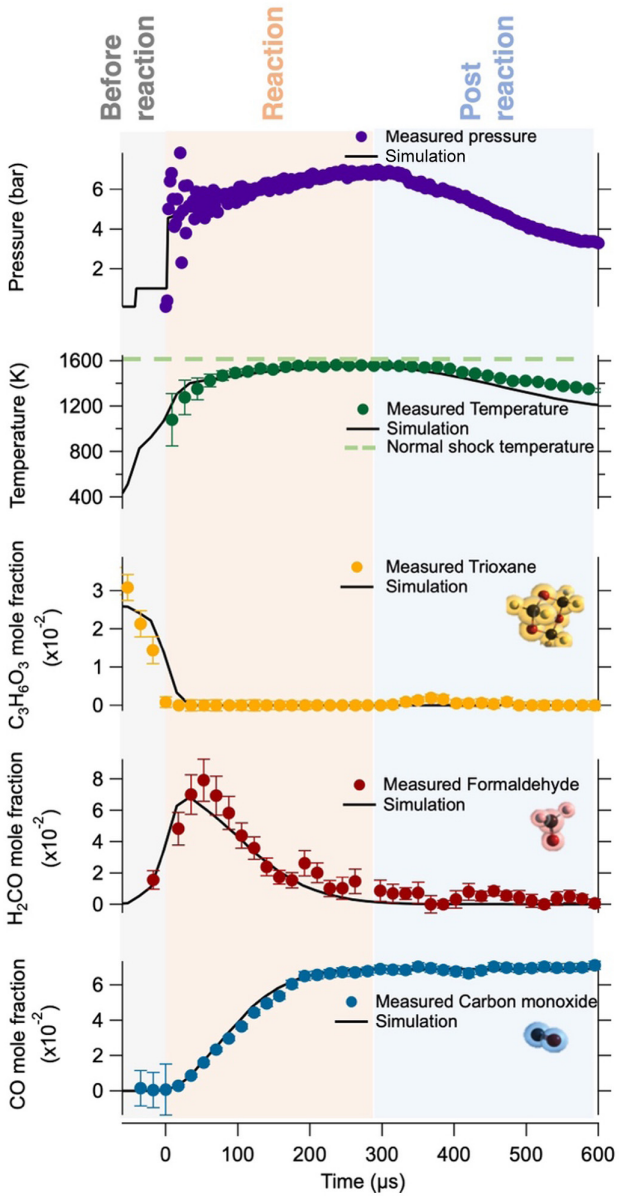

Fig. 4. Reaction time history. Comparison of DCS measurements and simulations for experiments with 2.6% $C_3H_6O_3$ in argon with reflected shock pressure 4.4 bar. Experimental temperature and mole fractions are two-point moving averages for clarity, Models are low-pass filtered with 17.5 μs time constant in line with experiments. Two high-uncertainty data points are removed from the H_2CO data trace at −17.5 and +17.5 μs due to poor fit convergence at low H_2CO concentration. Simulations are based on the kinetic model described in the text. Dashed green line shows the estimated temperature using frozen normal shock relations.

measure the decomposition of trioxane, access conditions sensitive to different formaldehyde chemical reactions compared to other studies, and reliably assign rate constants.

The robust architecture of the frequency combs and motionless design of dual-comb spectrometry represent a powerful platform that should be capable of compact, robust application in field situations in the future, particularly when combined with next generation chip-based frequency combs [50,51]. We expect this platform to generate high impact in the fields of physical chemistry, including combustion, hypersonic propulsion and re-entry,

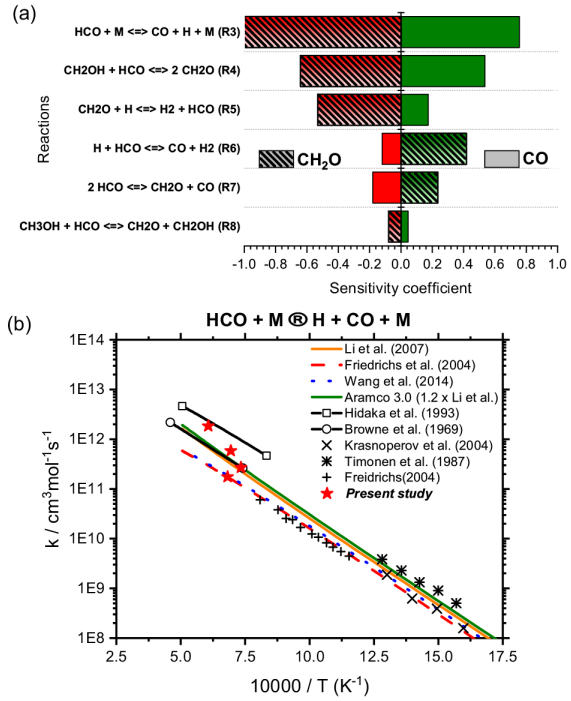

Fig. 5. (a) Sensitivity coefficient of each important reaction in the trioxane decomposition chemical mechanism to formaldehyde (H_2CO) and CO composition. The chemical system is most sensitive to the first reaction, and H_2CO and CO compositions are strongly correlated (opposite sensitivities). (b) Rate constants for $HCO + M \rightarrow H + CO + M$ derived from this work (red stars) compared to the literature.

planetary science, industrial monitoring, spectroscopy of novel quantum material, and bio-imaging [52–54].

Funding. National Science Foundation (1747774, 2016244, 2019195); Air Force Research Laboratory (FA8650-20-2-2418); Air Force Office of Scientific Research (FA9550-20-1-0328); National Institute of Standards and Technology.

Disclosures. The authors declare no conflicts of interest.

Data availability. Data are available upon reasonable request.

Supplemental document. See Supplement 1 for supporting content.

REFERENCES

1. M. P. Burke and S. J. Klippenstein, "Ephemeral collision complexes mediate chemically termolecular transformations that affect system chemistry," Nat. Chem. **9**, 1078–1082 (2017).
2. N. J. Labbe, R. Sivaramakrishnan, C. F. Goldsmith, *et al.*, "Weakly bound free radicals in combustion: "prompt" dissociation of formyl radicals and its effect on Laminar flame speeds," J. Phys. Chem. Lett. **7**, 85–89 (2016).
3. J. A. Miller, R. Sivaramakrishnan, Y. Tao, *et al.*, "Combustion chemistry in the twenty-first century: developing theory-informed chemical kinetics models," Prog. Energy Combust. Sci. **83**, 100886 (2021).
4. R. H. West and C. F. Goldsmith, "The impact of roaming radicals on the combustion properties of transportation fuels," Combust. Flame **194**, 387–395 (2018).
5. S. Schiller, "Spectrometry with frequency combs," Opt. Lett. **27**, 766–768 (2002).
6. I. Coddington, N. Newbury, and W. Swann, "Dual-comb spectroscopy," Optica **3**, 414–426 (2016).
7. G. Villares, A. Hugi, S. Blaser, *et al.*, "Dual-comb spectroscopy based on quantum-cascade-laser frequency combs," Nat. Commun. **5**, 5192 (2014).
8. Y. Yang, D. Burghoff, D. J. Hayton, *et al.*, "Terahertz multiheterodyne spectroscopy using laser frequency combs," Optica **3**, 499–502 (2016).

9. L. A. Sterczewski, J. Westberg, M. Bagheri, *et al.*, "Mid-infrared dual-comb spectroscopy with interband cascade lasers," Opt. Lett. **44**, 2113–2116 (2019).
10. P. Fjodorow, P. Allmendinger, R. Horvath, *et al.*, "Monitoring formaldehyde in a shock tube with a fast dual-comb spectrometer operating in the spectral range of 1740–1790 cm^{-1}," Appl. Phys. B **126**, 193 (2020).
11. N. H. Pinkowski, S. J. Cassady, C. L. Strand, *et al.*, "Quantum-cascade-laser-based dual-comb thermometry and speciation at high temperatures," Meas. Sci. Technol. **32**, 035501 (2021).
12. M. Yan, P.-L. Luo, K. Iwakuni, *et al.*, "Mid-infrared dual-comb spectroscopy with electro-optic modulators," Light Sci. Appl. **6**, e17076 (2017).
13. B. Jerez, P. Martín-Mateos, F. Walla, *et al.*, "Flexible electro-optic, single-crystal difference frequency generation architecture for ultrafast mid-infrared dual-comb spectroscopy," ACS Photonics **5**, 2348–2353 (2018).
14. P.-L. Luo, I.-Y. Chen, M. A. H. Khan, *et al.*, "Direct gas-phase formation of formic acid through reaction of Criegee intermediates with formaldehyde," Commun. Chem. **6**, 130 (2023).
15. D. A. Long, M. J. Cich, C. Mathurin, *et al.*, "Nanosecond time-resolved dual-comb absorption spectroscopy," Nat. Photonics **18**, 127–131 (2024).
16. S. Chaitanya Kumar, A. Esteban-Martin, T. Ideguchi, *et al.*, "Few-cycle, broadband, mid-infrared optical parametric oscillator pumped by a 20-fs Ti:sapphire laser," Laser Photonics Rev. **8**, L86–L91 (2014).
17. K. Iwakuni, G. Porat, T. Q. Bui, *et al.*, "Phase-stabilized 100 mW frequency comb near 10 μm," Appl. Phys. B **124**, 128 (2018).
18. G. Ycas, F. R. Giorgetta, E. Baumann, *et al.*, "High coherence mid-infrared dual comb spectroscopy spanning 2.6 to 5.2 microns," Nat. Photonics **12**, 202–208 (2018).
19. M. A. Abbas, Q. Pan, J. Mandon, *et al.*, "Time-resolved mid-infrared dual-comb spectroscopy," Sci. Rep. **9**, 17247 (2019).
20. A. J. Lind, A. Kowligy, H. Timmers, *et al.*, "Mid-infrared frequency comb generation and spectroscopy with few-cycle pulses and χ^2 nonlinear optics," Phys. Rev. Lett. **124**, 133904 (2020).
21. D. M. B. Lesko, H. Timmers, S. Xing, *et al.*, "A six-octave optical frequency comb from a scalable few-cycle erbium fibre laser," Nat. Photonics **15**, 281–286 (2021).
22. S. Vasilyev, A. Muraviev, D. Konnov, *et al.*, "Longwave infrared (6.6–11.4 μm) dual-comb spectroscopy with 240,000 comb-mode-resolved data points at video rate," Opt. Lett. **48**, 2273–2276 (2023).
23. B. J. Bjork, T. Q. Bui, O. H. Heckl, *et al.*, "Direct frequency comb measurement of OD + CO → DOCO kinetics," Science **354**, 444–448 (2016).
24. A. Barh, B. Ö. Alaydin, J. Heidrich, *et al.*, "High-power low-noise 2-GHz femtosecond laser oscillator at 2.4 μm," Opt. Express **30**, 5019–5025 (2022).
25. V. Smolski, S. Vasilyev, I. Moskalev, *et al.*, "Half-Watt average power femtosecond source spanning 3–8 μm based on subharmonic generation in GaAs," Appl. Phys. B **124**, 101 (2018).
26. T. Voumard, J. Darvill, T. Wildi, *et al.*, "1-GHz dual-comb spectrometer with high mutual coherence for fast and broadband measurements," Opt. Lett. **47**, 1379–1382 (2022).
27. J. H. Huh, Z. Chen, E. Vicentini, *et al.*, "Time-resolved dual-comb spectroscopy with a single electro-optic modulator," Opt. Lett. **46**, 3957–3960 (2021).
28. A. Dutt, C. Joshi, X. Ji, *et al.*, "On-chip dual-comb source for spectroscopy," Sci. Adv. **4**, e1701858 (2018).
29. G. Millot, S. Pitois, M. Yan, *et al.*, "Frequency-agile dual-comb spectroscopy," Nat. Photonics **10**, 27–30 (2015).
30. H. Tian, R. Li, L. A. Sterczewski, *et al.*, "Quasi-real-time dual-comb spectroscopy with 750-MHz Yb:fiber combs," Opt. Express **30**, 28427–28437 (2022).
31. N. Hoghooghi, S. Xing, P. Chang, *et al.*, "Broadband 1-GHz mid-infrared frequency comb," Light Sci. Appl. **11**, 264 (2022).
32. R. S. Tranter and P. T. Lynch, "A miniature high repetition rate shock tube," Rev. Sci. Instrum. **84**, 094102 (2013).
33. J. Zádor, C. A. Taatjes, and R. X. Fernandes, "Kinetics of elementary reactions in low-temperature autoignition chemistry," Prog. Energy Combust. Sci. **37**, 371–421 (2011).
34. K. Wang, R. Xu, T. Parise, *et al.*, "A physics-based approach to modeling real-fuel combustion chemistry–IV. HyChem modeling of combustion kinetics of a bio-derived jet fuel and its blends with a conventional Jet A," Combust. Flame **198**, 477–489 (2018).
35. Z. J. Buras, C. Safta, J. Zádor, *et al.*, "Simulated production of OH, HO2, CH2O, and CO2 during dilute fuel oxidation can predict 1st-stage ignition delays," Combust. Flame **216**, 472–484 (2020).
36. H. Chen, W. Ji, S. J. Cassady, *et al.*, "Using shock tube species time-histories in Bayesian parameter estimation: effective independent-data number and target selection," Proc. Combust. Inst. **39**, 5299–5308 (2023).
37. Y. Ding, S. Wang, and R. K. Hanson, "Sensitive and interference-immune formaldehyde diagnostic for high-temperature reacting gases using two-color laser absorption near 5.6 μm," Combust. Flame **213**, 194–201 (2020).
38. S. Xing, D. M. B. Lesko, T. Umeki, *et al.*, "Single-cycle all-fiber frequency comb," APL Photonics **6**, 086110 (2021).
39. N. R. Newbury, I. Coddington, and W. Swann, "Sensitivity of coherent dual-comb spectroscopy," Opt. Express **18**, 7929–7945 (2010).
40. N. Hoghooghi, R. K. Cole, and G. B. Rieker, "11-μs time-resolved, continuous dual-comb spectroscopy with spectrally filtered mode-locked frequency combs," Appl. Phys. B **127**, 17 (2021).
41. P. T. Lynch and G. Wang, "Chemical thermometry in miniature HRRST using 1,1,1-trifluoroethane dissociation," Proc. Combust. Inst. **36**, 307–314 (2017).
42. J. Mandon, G. Guelachvili, and N. Picqué, "Fourier transform spectroscopy with a laser frequency comb," Nat. Photonics **3**, 99–102 (2009).
43. R. K. Cole, A. S. Makowiecki, N. Hoghooghi, *et al.*, "Baseline-free quantitative absorption spectroscopy based on cepstral analysis," Opt. Express **27**, 37920–37939 (2019).
44. I. E. Gordon, L. S. Rothman, R. J. Hargreaves, *et al.*, "The HITRAN2020 molecular spectroscopic database," J. Quant. Spectrosc. Radiat. Transfer **277**, 107949 (2022).
45. K. Sun, S. Wang, R. Sur, *et al.*, "Time-resolved in situ detection of CO in a shock tube using cavity-enhanced absorption spectroscopy with a quantum-cascade laser near 4.6 μm," Opt. Express **22**, 24559–24565 (2014).
46. W. Tang and K. Brezinsky, "Chemical kinetic simulations behind reflected shock waves," Int. J. Chem. Kinet. **38**, 75–97 (2006).
47. C.-W. Zhou, Y. Li, U. Burke, *et al.*, "An experimental and chemical kinetic modeling study of 1,3-butadiene combustion: ignition delay time and laminar flame speed measurements," Combust. Flame **197**, 423–438 (2018).
48. M. Demireva, J. Oreluk, A. L. Dewyer, *et al.*, "Genetic algorithm optimization of a master equation cyclopentane oxidation model against time-resolved speciation experiments," Combust. Flame **257**, 112506 (2022).
49. Q. Liang, Y.-C. Chan, P. B. Changala, *et al.*, "Ultrasensitive multispecies spectroscopic breath analysis for real-time health monitoring and diagnostics," Proc. Natl. Acad. Sci. USA **118**, e2105063118 (2021).
50. M. Yu, Y. Okawachi, A. G. Griffith, *et al.*, "Silicon-chip-based mid-infrared dual-comb spectroscopy," Nat. Commun. **9**, 1869 (2018).
51. C. Bao, Z. Yuan, H. Wang, *et al.*, "Interleaved difference-frequency generation for microcomb spectral densification in the mid-infrared," Optica **7**, 309–315 (2020).
52. E. A. Muller, B. Pollard, H. A. Bechtel, *et al.*, "Nanoimaging and control of molecular vibrations through electromagnetically induced scattering reaching the strong coupling regime," ACS Photonics **5**, 3594–3600 (2018).
53. H. Tu, Y. Liu, D. Turchinovich, *et al.*, "Stain-free histopathology by programmable supercontinuum pulses," Nat. Photonics **10**, 534–540 (2016).
54. M. Hermes, R. B. Morrish, L. Huot, *et al.*, "Mid-IR hyperspectral imaging for label-free histopathology and cytology," J. Opt. **20**, 023002 (2018).